CHEMIJA. 2015. Vol. 26. No. 3. P. 175–183

The self-healing ability of cerium oxide films on carbon steel

O. Girčienė*,

L. Gudavičiūtė,

A. Selskis,

V. Jasulaitienė,

S. Šakirzanovas,

R. Ramanauskas

Institute of Chemistry,
Centre for Physical
Sciences and Technology,
Goštauto St. 9,
LT-01108 Vilnius, Lithuania

Active corrosion protection of metals implies not only mechanical covering of the protected surface with a dense barrier coating, but also provides self-healing properties, which allow durable protection even after partial damage of the coating. The aim of the present study was to develop the deposition process of a chrome-free conversion coating on carbon steel and to study its self-healing capacities. The amorphous phosphate coating on carbon steel was chosen as the base for deposition of the cerium oxide films. The SEM, XRD and XPS techniques were applied for the structural, phase and composition characterization of the investigated coatings, voltametric measurements were carried out to determine the passive layer protective ability, while EIS studies yielded information on the self-healing properties of different protective systems affected by introduced artificial defects. The carbon steel and the phosphated carbon steel surfaces were modified with Ce ions by deposition of Ce films from the $Ce(NO_3)_3$ solution without and with SO_4^{2-} ions. The presence of the SO_4^{2-} ions in the conversion solution resulted in formation of the film, containing a larger amount of Ce, with respect to the pure $Ce(NO_3)_3$ solution and a higher amount of Ce^{4+} in the film. However, a low conversion films thickness and the presence of cracks yielded a lower level of steel corrosion protection. The increase of the low frequency impedance during immersion of the samples with a cerium film can be correlated to the active corrosion protection originating the self-healing of defects.

Key words: carbon steel, phosphate coating, cerium oxide film, self-healing

INTRODUCTION

Carbon steel is widely used in industry; however, its susceptibility to corrosion in many environments limits its applications. Therefore a wide variety of coating processes have been developed in the past to achieve coatings with desirable properties to meet certain surface requirements. For years, chromating has been applied to produce corrosion resistant conversion layers onto different substrates. Chromate chemical conversion films have high corrosion and wear resistance due to self-healing capacity of the film resulting from the dissolution (oxidation capacities) of Cr(VI) ions. Unfortunately, chromate compounds are remarkably toxic and carcinogenic and dissolved Cr(VI) ions have an environmental impact on humans; consequently, alternative surface treatment technologies are required.

The replacement of chromate conversion layers by a new generation of conversion coatings called "environmentally friendly" has been strongly stimulated in the last years and non-chromate coatings, such as phosphate [1–4], molybdate [5–8] and other based materials [9, 10], have been studied. Chromate conversion coatings have unrivalled self-healing abilities, which are believed to arise from the migration of a soluble Cr(VI) compound in the coating to a scratch or defect, where they are reduced to form a new protection layer [11]. Self-healing is defined as the ability of material or surface to automatically heal or repair damages. Rare earth metal ions, such as cerium, lanthanum, and yttrium, have been recognized as an effective corrosion inhibitor for some aluminum alloys in a chloride-containing solution [12]. In a series of studies on the use of cerium ion in protective coatings, Hinton and Wilson [13] reported that the cerium ion, which acts as an inhibitor in solution, was as effective as the chromium ion. The action of the cerium ion resembled that of the chromium ion, and CeO_2 acted as a barrier film. When a defect was generated, a cerium ion in the film repaired it, due to dissolution from the film and oxidation of the defect site [14]. The study of cerium based conversion coatings on galvanized steel have shown the influence of anions, such as Cl^-, NO_3^-, SO_4^{2-}, CH_3COO^-, in a coating deposition solution

* Corresponding author. E-mail: olgag@chi.lt

on the corrosion behavior of the formed film [15]. The results of the electrochemical measurement and the salt spray test indicate that the corrosion behavior was greatly improved by the addition of SO_4^{2-} to the coating solution. It was supposed that the presence of SO_4^{2-} in the solution forms a complex between Ce^{3+} and SO_4^{2-}, which causes the incorporation of SO_4^{2-} into the cerium conversion coatings [16]. At the same time the lack of data on the protective abilities of cerium based conversion coatings on the steel surface can be stated.

The aim of the present study was to develop the deposition process of a chrome-free conversion coating on carbon steel and to study its self-healing capacities.

EXPERIMENTAL

Materials and sample preparation

Carbon steel specimens, 10 × 20 mm and 1 mm thick with an area of 4 cm^2 previously polished with emery paper up to grade 400, degreased with ethanol and rinsed with distilled water, were used as base metal electrodes. The following samples for comparison of their corrosion behaviour were investigated: polished carbon steel (CS), carbon steel coated with amorphous Fe phosphate (FeP) and CS and FeP with cerium conversion coatings (Ce1 and Ce2).

The phospating solution was used for amorphous FeP coating formation: 0.15 M H_3PO_4, 0.003 M $H_2C_2O_4$, 0.001 M Na_2MoO_4, pH = 4–5, 50 °C, 10 min.

Ce1 and Ce2 conversion coatings were formed by simple immersion of the CS and FeP samples for 24 h at 25 °C into solutions containing 0.05 M $Ce(NO_3)_3$ and 0.05 M $Ce(NO_3)_3$ + 0.025 M Na_2SO_4, respectively.

Electrochemical measurements

The corrosion behaviour of samples was investigated in an aerated stagnant 0.5 M NaCl solution. The electrolyte was prepared from analytical grade chemicals and deionized water.

All electrochemical measurements were performed at ambient temperature with an Autolab PGSTAT302 potentiostat using a standard three-electrode system with a Pt counter electrode and a saturated Ag/AgCl reference electrode. All potentials are reported versus the saturated Ag/AgCl reference electrode. The corrosion current densities (i_{corr}) were determined by Tafel line extrapolation. One specimen was used for a measurement, with the potential scan rate of 0.5 mV s^{-1}, from the cathodic to anodic region.

The measurements of electrochemical impedance spectra (EIS) were performed at the open circuit potential with the FRA2 module applying a signal of 10 mV amplitude in the frequency range 20 kHz to 0.001 Hz. The data obtained were fitted and analysed using the EQUIVCRT program of Boukamp [17].

Morphology and composition

The phase composition and crystallinity of the phosphate coatings were determined by X-ray diffraction (XRD) measurements, which were performed with a diffractometer D8 Advance (Bruker AXS) equipped with the Göbel mirror (primary beam monochromator) for Cu radiation (λ = 0.154183 nm). The step-scan mode was used in the 2Θ ranges from 5° to 50° with a step-length of 0.04° and a counting time of 5 s per step.

A microstructure and elemental composition of specimens were studied by a scanning electron microscope (SEM). A Helios NanoLab 650 dual beam workstation (FEI) with an X-Max 20 mm^2 energy dispersive detector (energy resolution of 127 eV for Mn K_α, Oxford Instruments) was used for imaging and energy dispersive analysis. The element mappings were carried out under the following measurement conditions: accelerating voltage, 8 kV, beam current, 3.2 nA, mapping resolution, 512 × 352 pixels. X-ray line K_α (Si) was used for the characterization of element distribution on the sample surface. The deposited film thickness analysis was performed on by the focused ion beam (FIB) technique produced and vacuum Pt coated cross-sections of samples.

The X-ray photoelectron spectroscopy (XPS) studies were performed by a spectrometer ESCALAB using X-radiation of MgK_α (1253.6 eV, pass energy of 20 eV). To obtain depth profiles, the samples were etched in the preparation chamber by ionised argon at a vacuum of 5×10^{-4} Pa. An accelerating voltage of ca. 1.0 kV and a beam current of 20 μA cm^{-2} were used.

RESULTS AND DISCUSSION

Phosphate conversion coating

Active corrosion protection of metals implies not only mechanical covering of the protected surface with a dense barrier coating, but also provides self-healing properties, which allow durable protection even after partial damage of the coating. These properties can be achieved by introducing of specific corrosion inhibitors into the coating system. The phosphate coating FeP on the steel surface was chosen as the base for the active corrosion protection film.

The FeP coating was formed in the solution which did not contain any other coating constituting metal ions but only the acid phosphates of potassium. This coating consists of a mixture of iron phosphate and iron oxide and is generally regarded as being amorphous. According to Machu [18] the reaction proceeds in the three stages:

$$Fe + NaH_2PO_4 + 2H_2O + O_2 \rightarrow 2Fe(H_2PO_4)_2 + 4NaOH, \quad (1)$$

$$2Fe(H_2PO_4)_2 + 2NaOH + O \rightarrow 2Fe(PO_4)_2 + 2NaH_2PO_4, \quad (2)$$

$$2Fe(H_2PO_4)_2 + 6NaOH + O \rightarrow$$
$$2Fe(OH)_3 + 2NaH_2PO_4 + 2Na_2HPO_4 + H_2O. \quad (3)$$

Finally, ferric hydroxide decomposes into an insoluble ferric oxide:

$$2Fe(OH)_3 \rightarrow Fe_2O_3 + 3H_2O. \quad (4)$$

All the insoluble products go into the coating and the solutions operate sludge-free.

According to XRD measurements the CS sample covered with the FeP exhibited only peaks corresponding to Fe, which confirms the amorphous structure of the coating (Fig. 1).

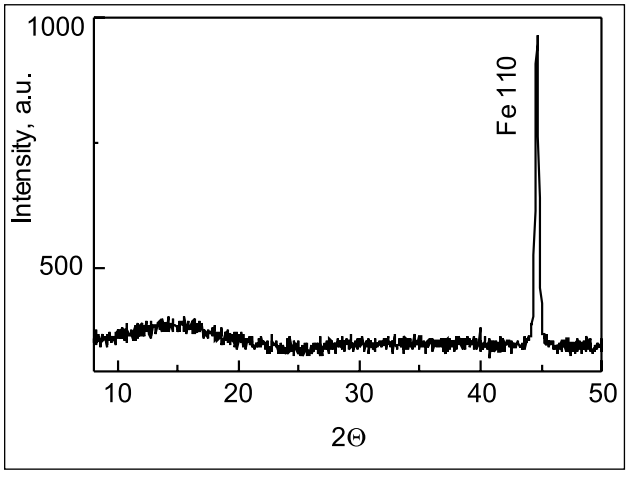

Fig. 1. XRD patterns of phosphated carbon steel (FeP)

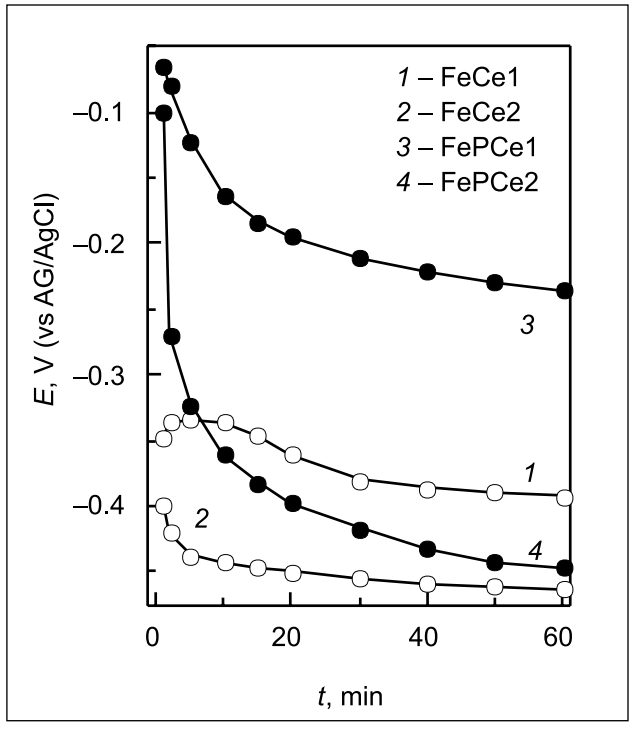

Fig. 2. Alteration of CS (*1*, *2*) and FeP (*3*, *4*) potentials in time during immersion in solutions: *1*, *3* – 0.05 M $Ce(NO_3)_3$, *2*, *4* – 0.05 M $Ce(NO_3)_3$ + 0.025 M Na_2SO_4, 25 °C

Cerium conversion coatings

Specific corrosion inhibitors which were introduced into the FeP coating system were Ce ions. When the metallic substrates are immersed into the conversion bath (pH ~5.5), the dissolution of the outer oxide layers is taking place [19]. This leads to the formation of cathodic activity and production of hydroxyl ions. Thus, Ce^{3+} precipitates as hydroxides:

$$Ce^{3+} + 3OH^- \rightarrow Ce(OH)_3\downarrow. \quad (5)$$

With increasing treatment time the cerium conversion film became richer in Ce(IV) species [19]. This evolution shows that hydroxides are converted into oxides, or that oxides precipitate preferentially. The conversion of $Ce(OH)_3$ into CeO_2 has been mentioned in literature [20]. The presence of Ce(IV) could be due to the dismutation solid state reaction [19, 20]:

$$Ce(OH)_3 \rightarrow CeO_2 + H_2O + ½\ H_2. \quad (6)$$

Figure 2 shows an alteration of CS and FeP samples potentials during the immersion in the 0.05 M $Ce(NO_3)_3$ (Ce1) and 0.05 M $Ce(NO_3)_3$ + 0.025 M Na_2SO_4 (Ce2) solutions. The most rapid *E* evolution for CS occurred within ~20–30 min, while further potential evolution was slower and did not change significantly. The values of the stable CS potential plateau were achieved after ~1 h.

In the case of FeP samples Ce-based passivation took a longer period of time and the equilibrium state in the system was obtained after more than 1 hour (Fig. 2). More reproducible data were obtained when Ce based passivation continued for 24 h.

Composition and morphology

SEM images of the surface morphology and cross sections of conversion Ce coatings formed on CS (FeCe1, FeCe2) and on FeP (FePCe1, FePCe2) are presented in Figs. 3 and 4. The surface of FeCe samples (Fig. 3a, c) reflects the morphology of the base steel surface with the random located crystallite aggregates, which can be supposed to be precipitated Ce oxide compounds according to Eqs. (5) and (6). The SEM images of cross-sections of these samples (Fig. 3b, d) indicate a dual structure of the conversion FeCe films, while those of FeCe2 formed in the sulphate containing a solution (Fig. 3d) were thinner (~200 nm), with respect to the FeCe1 film (Fig. 3b), formed in a pure $Ce(NO_3)_3$ solution (~300 nm). The surface of FePCe samples exhibited the presence of structural defects like cracks and pores (Fig. 4a, c), which are characteristic of phosphate coatings, while the thickness of the modified films was close to 1 μm (Fig. 4b, d), which is typical of such films, and which implies the interaction of FeP with Ce ions on the outside of the film and Ce compounds located on the top of the film.

The analysis of elemental composition of the investigated conversion films was performed by EDS measurements, the results of which are listed in Table 1 and indicate that all conversion layers were thin enough, as the most intensive signal

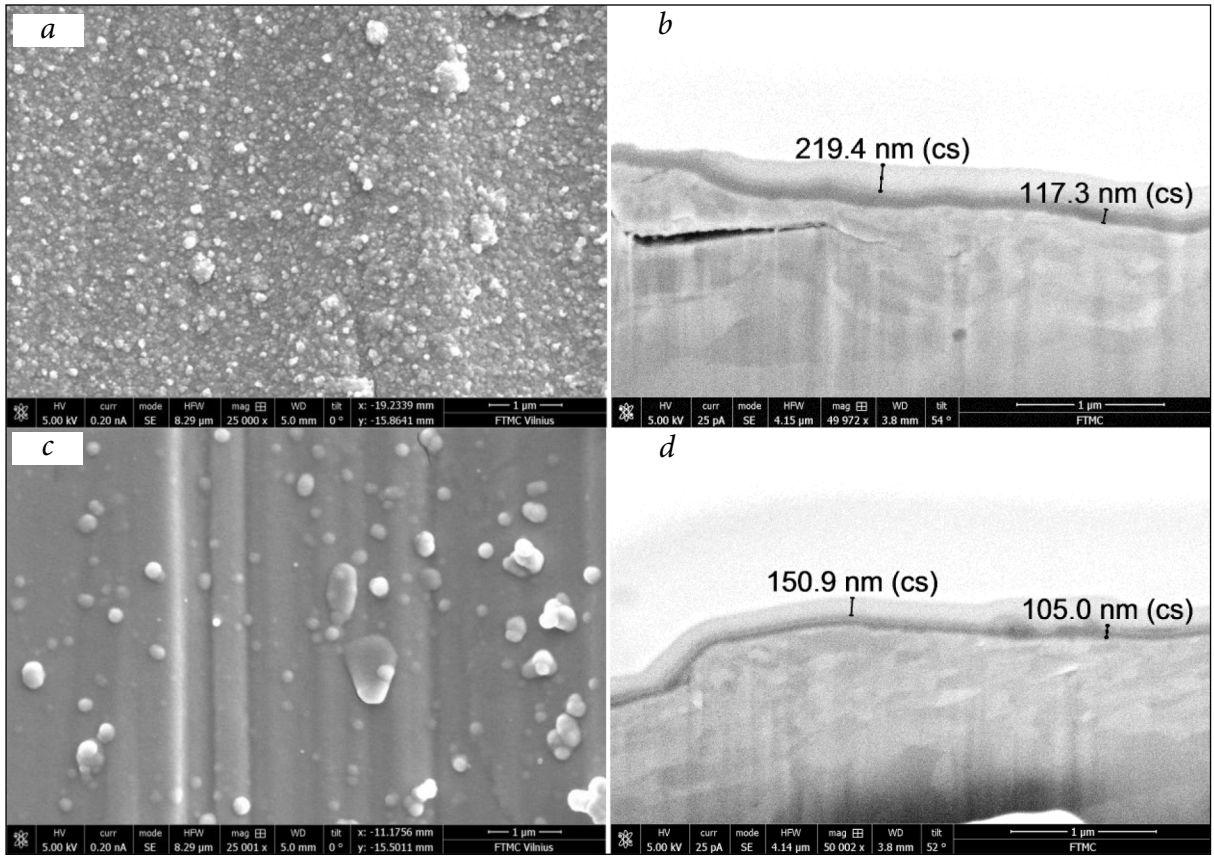

Fig. 3. SEM images of CS treated with (*a*, *b*) 0.05 M $Ce(NO_3)_3$ (FeCe1) and (*c*, *d*) 0.05 M $Ce(NO_3)_3$ + 0.025 M Na_2SO_4 (FeCe2) for 24 h

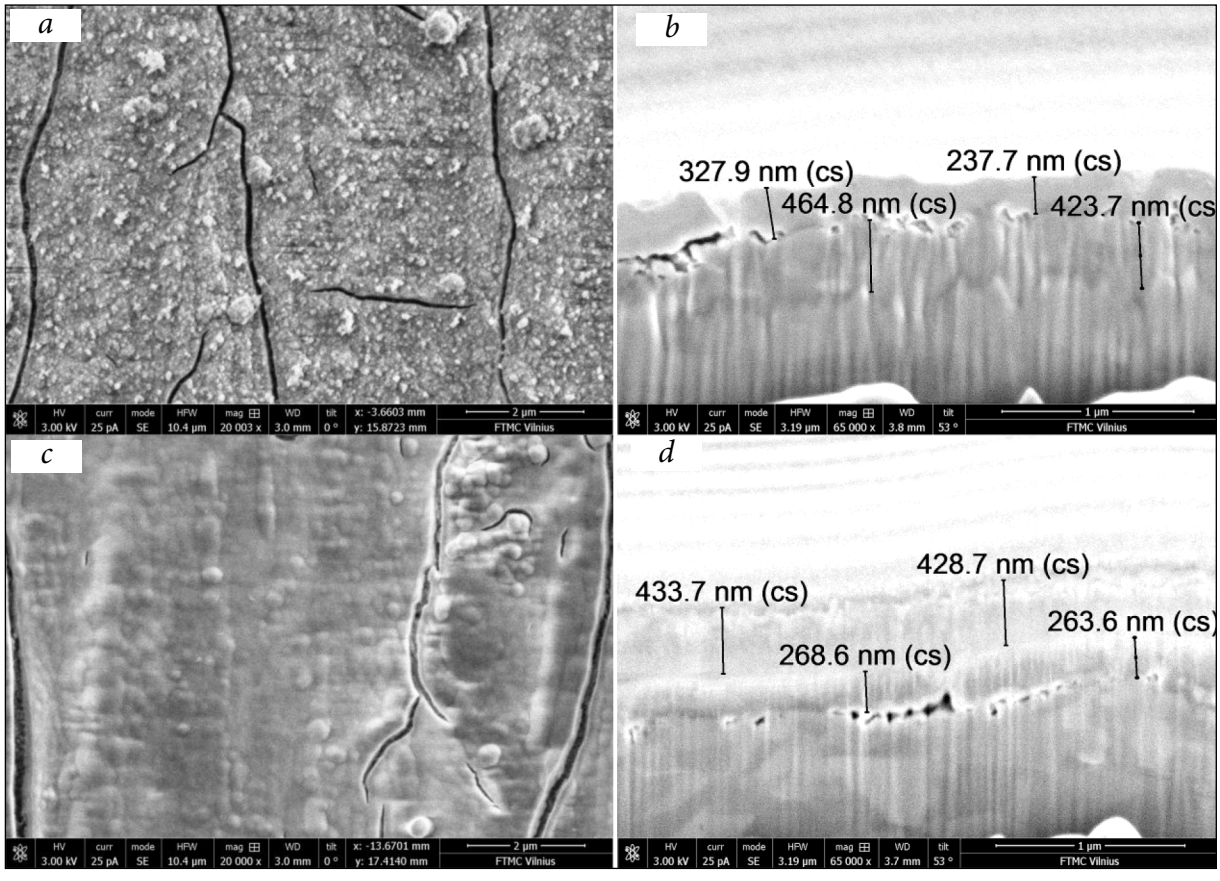

Fig. 4. SEM images of FeP treated with (*a*, *b*) 0.05 M $Ce(NO_3)_3$ (FePCe1) and (*c*, *d*) 0.05 M $Ce(NO_3)_3$ + 0.025 M Na_2SO_4 (FePCe2) for 24 h

was observed from the base Fe metal. The next dominant element constituting films is O, and the fact that the amount of P both in a pure phosphate film and a modified one with Ce was close to 1 at.% implies that Fe oxides are one of the principal constituents of the formed conversion films. The amount of Ce in the coatings varied from 1 to 2 at.% and was detected to be slightly higher for the samples formed in the solution containing sulphate ions. Besides, the film formed in the solution containing sulphate ions additionally contained ~2 at.% of S (FeCe2, FePCe2).

Table 1. **The elemental composition of the surface of the investigated samples**

Sample	Elements, at.% (by EDS)				
	O	P	Fe	Ce	S
CS	7.9	–	92.1	–	–
FeP	19.8	0.9	79.3	–	–
FeCe1	28.4	–	70.2	1.4	–
FeCe2	39.2	–	56.4	2.3	2.1
FePCe1	36.7	1.4	60.8	1.1	–
FePCe2	39.0	1.2	56.2	1.7	1.9

The composition and the oxidation state of Ce on the CS and FeP surface were examined using XPS measurements (Table 2). It is worthy of note that the Ce 3d spectra of CS and FeP samples coated with cerium are identical. The Ce 3d spectra of FeP with Ce1 and Ce2 coatings are presented in Fig. 5. In the Ce 3d region three different zones are observed. The first corresponds to the peaks that appear in the binding energy range from 880 to 890 eV due to Ce $3d_{5/2}$, the second includes the zone where the Ce $3d_{3/2}$ and Ce $3d_{5/2}$ spectra overlap for the binding energies from 890 to 910 eV, and the third one is due to the emergence of the satellite peak associated with Ce $3d_{3/2}$ at an energy of 917 eV. This peak is of crucial importance for determination of the oxidation state of cerium because its presence is only associated with Ce^{4+} [21, 22]. The Ce 3d spectra for all the investigated samples were similar to each other (Fig. 5), and there was a peak at 916.3 eV characteristic of Ce^{4+} [23].

Table 2. **XPS analysis data of the investigated samples (10 nm depth)**

Sample						
	Fe	O	P	Ce	N	S
FeCe1	6.7	63.1	–	29.2	1.0	–
FeCe2	3.8	53.8	–	35.0	1.6	5.8
FePCe1	7.5	59.6	1.6	28.4	2.9	–
FePCe2	3.1	52.7	1.1	36.2	2.7	4.2

Paying attention to the element, which may be responsible for the self-healing capability of conversion films, the oxidation states of Ce were analysed. The percentage area of Ce^{4+} on the sample surface was calculated from the equation [24–26]:

$$Ce^{4+}\% = \mu\%/14 \times 100, \quad (7)$$

where μ is the satellite area percentage at 916.3 eV with respect to the total Ce 3d area. Table 3 shows the quantity of Ce^{4+} % at 5 nm and 10 nm depths. The percentage of Ce^{4+} to total Ce for the FeCe1 and FePCe1 samples was 22.1% and 27.2%, respectively, while for the FeCe2 and FePCe2 samples it was equal to 49.1% and 39.5%, respectively, at a depth of 10 nm (Table 3). It implies that the presence of SO_4^{2-} ions in the Ce conversion film solution enhances the formation of Ce of a higher oxidation state. Meanwhile, the Ce^{3+} and Ce^{4+} compounds were identified in all the investigated cerium films on CS and FeP, but the amount of Ce^{4+} was higher in the FeCe2 and FePCe2 samples.

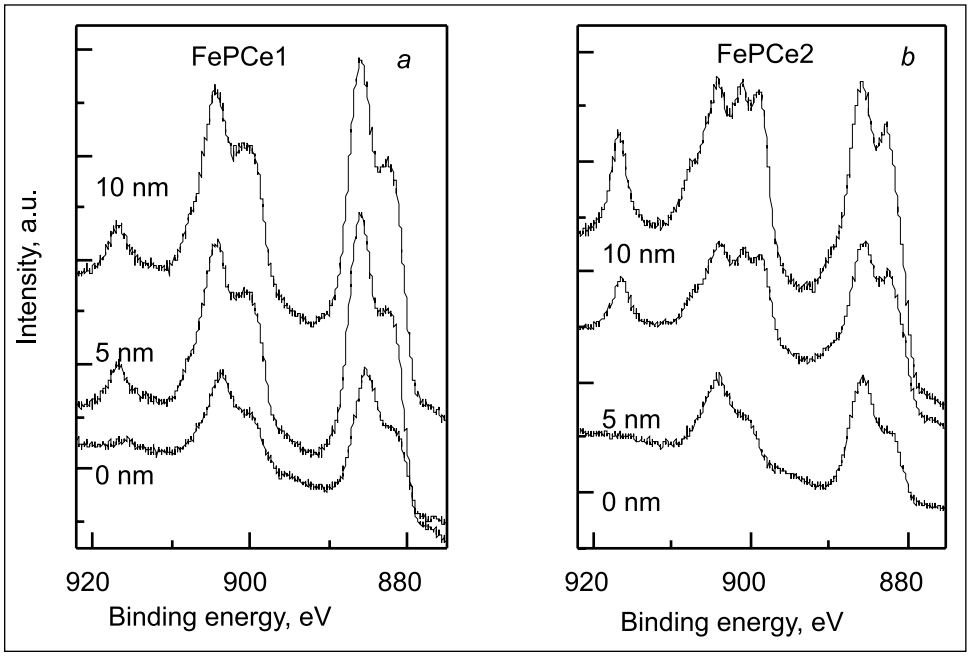

Fig. 5. XPS spectra for the Ce3d region obtained on FePCe1 (*a*) and FePCe2 (*b*)

Table 3. **The area percentage of Ce^{4+} at different depths calculated from XPS data**

Depth, nm	Ce^{4+} concentration, %			
	FeCe1	FeCe2	FePCe1	FePCe2
5	22.8	41.3	19.6	43.5
10	22.1	49.1	27.2	39.5

Self-healing ability

The impedance spectra can be used to provide adequate modelling of the physicochemical processes on the coated substrate during corrosion tests, besides, EIS can effectively be employed as a routine method to study self-healing properties of different protective systems affected by introduced artificial defects [27, 28]. An evolution of the EIS spectra for the FeCe1 sample in a 0.5 M NaCl solution is presented in Fig. 6. The Bode plot for FeCe1 before defect formation has two well-defined time constants. A resistive plateau at 10^2–10^4 Hz represents the resistance of the solution and the pore resistance of this coating, while the time constant at the lowest frequencies (0.01–1 Hz) is related to the corrosion activity. A fast drop in impedance at low frequencies occurs when an artificial defect is created in the Ce1 coating. Artificial scratches were made by a sharp metallic needle. This drop is related to the breakdown of the oxide film when the corrosion process began on the naked metal surface. However, after 1 h period of time the impedance starts rising again towards the initial values (Fig. 6). The increase in low frequency impedance can be related to the partial recovery of the oxide film and suppression of the corrosion activity in the defect [27, 28].

Bode plots for the Ce1 conversion coating on FeP during the immersion in 0.5 M NaCl before and after defect formation are given in Fig. 7. A drop in impedance at low frequencies occurs when an artificial defect is made in the

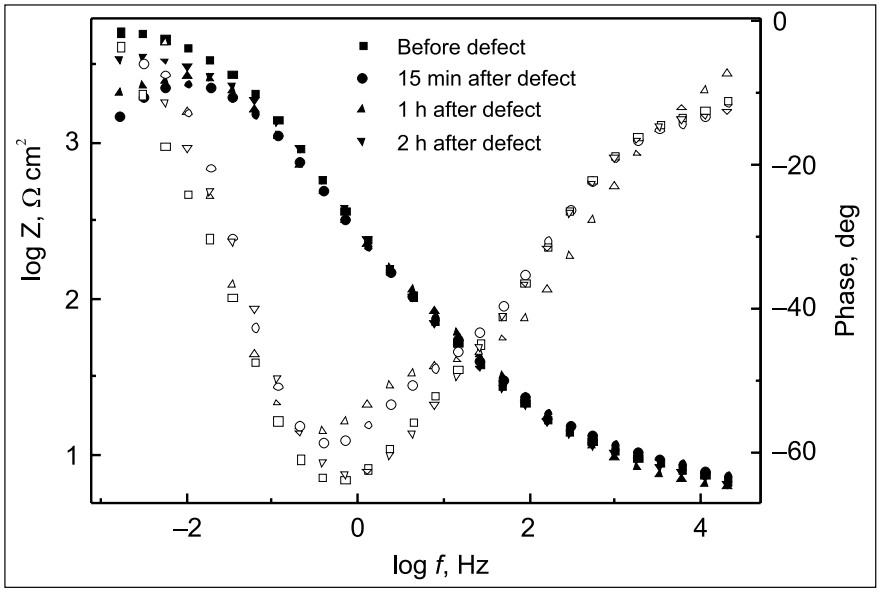

Fig. 6. Impedance spectra during FeCe1 immersion in 0.5 M NaCl before and after defect formation

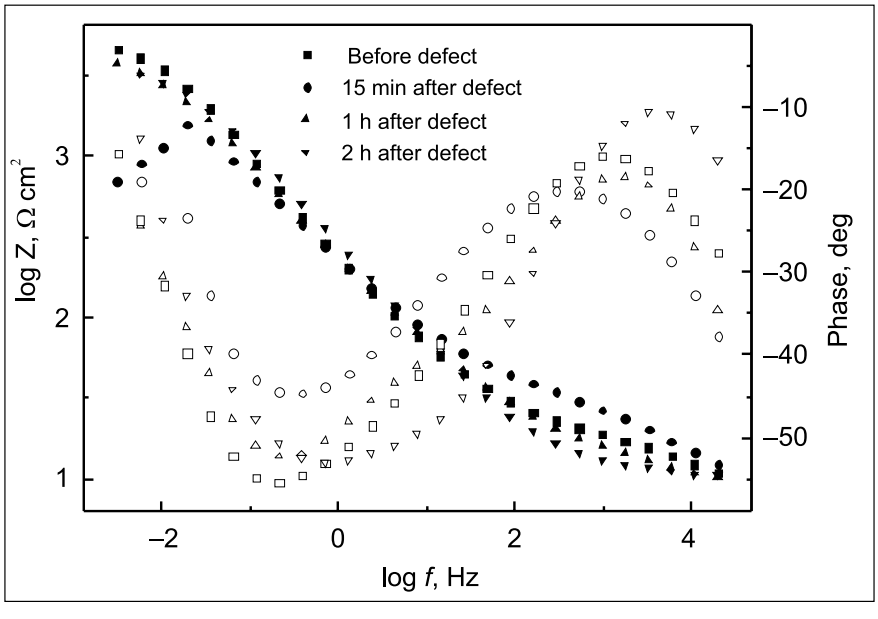

Fig. 7. Impedance spectra during FePCe1 immersion in 0.5 M NaCl before and after defect formation

coating. After 1 h the impedance at low frequencies starts rising again towards the initial values, while the impedance of high frequencies after defect formation tends to continue the decrease for long immersion. The low frequency impedance value is the same as that before the scratch formation after 2–3 h of immersion in the chloride solution.

The increase of the low frequency impedance suggests that both the FeCe1 and FePCe1 conversion films provide active corrosion protection.

Protective ability

The corrosion behaviour of CS and FeP samples with Ce1 and Ce2 coatings was investigated by the linear polarization and EIS measurements, which were carried out in a 0.5 M NaCl solution. The data obtained have shown that corrosion potential E_{corr} values of all samples with conversion coatings exhibited more positive potentials as compared to those of bare steel (Table 4). The FeCe1 and FeCe2 samples exhibited ~50 mV, while FePCe1 and FePCe2 ~80 mV exhibited more positive potentials as compared to that of CS.

Table 4. **The electrochemical parameters (corrosion current density i_{corr}, corrosion potential E_{corr}, polarization resistance R_p) and protection efficiency P% of the investigated samples determined in a 0.5 M NaCl solution**

Sample	Electrochemical parameters				
	E_{corr}, V (vs Ag/AgCl)	i_{corr}, A cm^{-2}	P% by Eq. (8)	R_p, kΩ cm^2	P% by Eq. (9)
CS	–0.609	$5.3 \cdot 10^{-6}$	–	0.95	–
FeCe1	–0.556	$1.6 \cdot 10^{-6}$	69.8	3.31	72.5
FeCe2	–0.555	$1.7 \cdot 10^{-6}$	67.9	2.20	56.8
FeP	–0.588	$3.1 \cdot 10^{-6}$	41.5	1.65	42.4
FePCe1	–0.525	$1.4 \cdot 10^{-6}$	73.6	3.53	73.1
FePCe2	–0.524	$1.6 \cdot 10^{-6}$	69.8	2.94	67.8

The polarization curves of the investigated samples are shown in Fig. 8. The values of the i_{corr} were determined from polarization measurements and the results obtained are listed in Table 4. As seen from the data, all samples coated with cerium exhibited the lowest values of i_{corr}, which varied in a narrow range of $1.4–1.7 \cdot 10^{-6}$ A cm^{-2}. The protection efficiency P% of samples was calculated by the Equation [16, 21]:

$$P\% = (i^{o}_{corr} - i_{corr})/i^{o}_{corr} \times 100, \quad (8)$$

where i^{o}_{corr} and i_{corr} denote the corrosion current density of bare steel and that of the electrode with the conversion coating, respectively. The calculated values of P% increased from 41.5% for FeP sample up to ~70–74% for all samples coated with Ce1 or Ce2. The highest P% values reached 73%

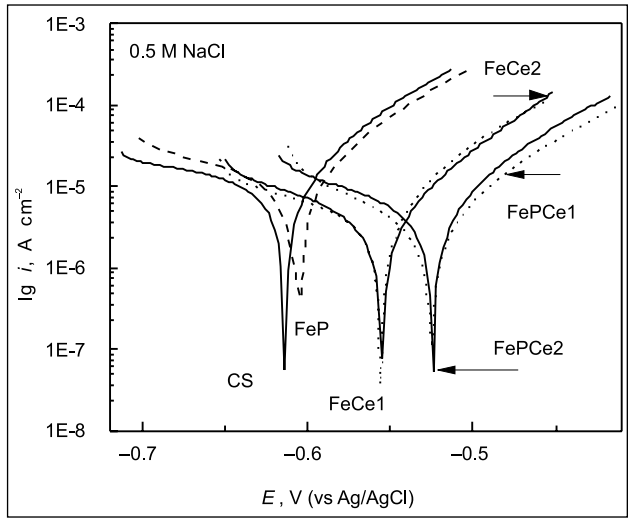

Fig. 8. Potentiodynamic polarization curves of the samples measured in a 0.5 M NaCl solution at 25 °C, 0.5 mV s^{-1}

and were stated for FeCe1 and FePCe1 coatings (Table 4). Therefore, it can be stated that the Ce1 conversion film formed in the solution free from sulphate ions increased the corrosion resistance of CS and FeP to a greater extent than Ce2 films formed in the sulphate containing solution.

EIS diagrams for the investigated samples exposed to a 0.5 M NaCl solution for 0.5 h are given in Figs. 9 and 10. The data obtained were fitted and analysed using the EQUIVCRT program of Boukamp [17]. To interpret the EIS data, the $R_1(Q_1[R_2(R_3Q_2)])$ equivalent circuit model, that is generally used to describe corrosion processes, was applied. The calculated parameters of equivalent circuit were used for the simulation of impedance diagrams (Table 5). The polarization resistance ($R_p = R_1 + R_2 + R_3$) values of the investigated samples are listed in Table 4. FeP sample possessed ~1.5 fold, whereas FeCe1 and FePCe1 had ~3.5 fold higher R_p values, respectively, as compared with those of CS.

The protection efficiency P% of coatings was calculated using the following Equation [2]:

$$P\% = (R_p - R_{pm})/R_p \times 100, \quad (9)$$

where R_{pm} and R_p denote the polarization resistance of bare steel and that of the electrode with the conversion coating, respectively. The results obtained imply that the samples with the Ce1 conversion coating (FeCe1 and FePCe1) demonstrated better protective properties (P% = 73%) in a 0.5 M NaCl solution (Table 4).

The FeCe2 and FePCe2 films were supposed to exhibit better protective abilities with respect to the FeCe1 and FePCe1 samples, because a higher amount of less soluble Ce (IV) compounds according to XPS measurements was detected for these samples. However, a low conversion films thickness and the presence of cracks in the samples (Figs. 4 and 5) yielded a lower level of steel corrosion protection.

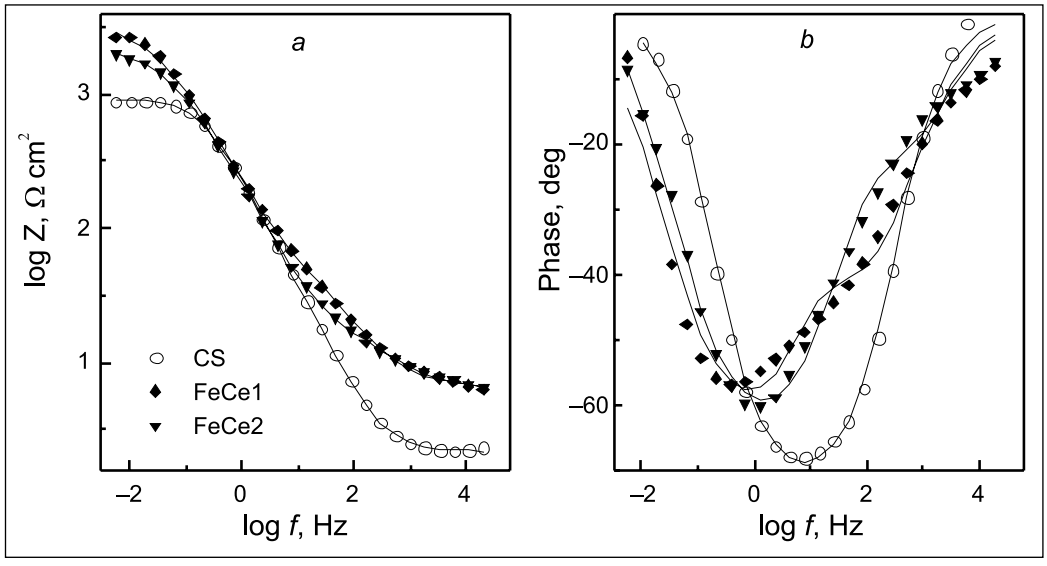

Fig. 9. Bode plots of EIS spectra after immersion of CS samples without/with cerium films into a 0.5 M NaCl solution

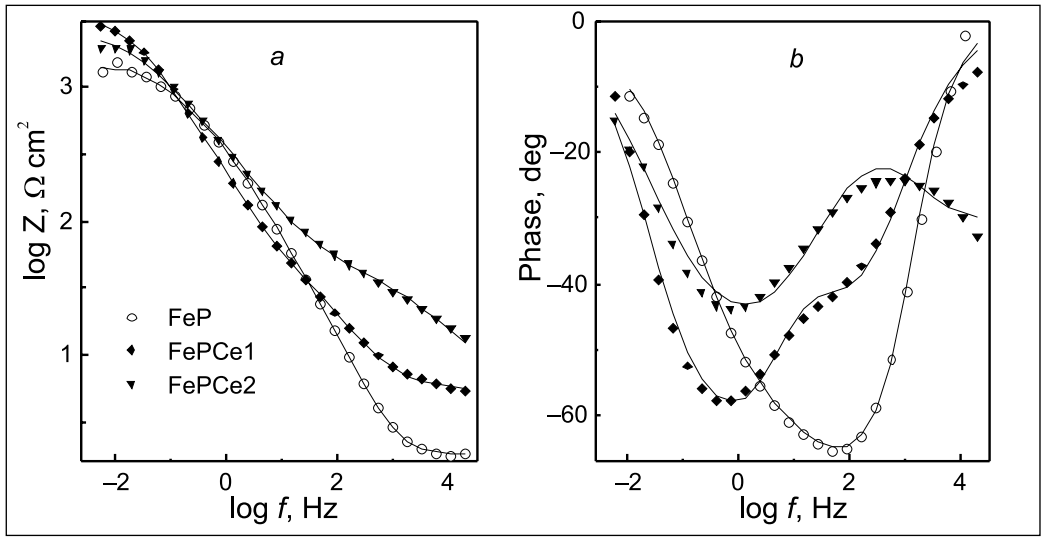

Fig. 10. Bode plots of EIS spectra after immersion of FeP samples without/with cerium films into a 0.5 M NaCl solution

Table 5. **EIS parameters obtained by fitting the Bode plots (Figs. 9 and 10) with equivalent circuit $R_1(Q_1[R_2(R_3Q_2)])$ for the investigated samples**

Sample	R_1, Ω cm²	R_2, Ω cm²	$Y_0(Q_1)/10^{-5}\Omega^{-1}$ cm^{-2} s^n	$n(Q_1)$	R_3, kΩ cm²	$Y_0(Q_2)/10^{-5}\Omega^{-1}$ cm^{-2} s^n	$n(Q_2)$
CS	2	–	–	–	0.95	89.3	0.82
FeCe1	6	81	65.9	0.69	3.23	47.4	0.79
FeCe2	6	14	44.1	0.71	2.18	75.1	0.76
FeP	2	4	7.3	0.99	1.64	77.6	0.61
FePCe1	5	81	68.2	0.68	3.45	49.8	0.80
FePCe2	2	52	25.5	0.50	2.88	72.4	0.60

CONCLUSIONS

Carbon steel and the phosphated carbon steel surfaces were modified with Ce ions by deposition of Ce films from the $Ce(NO_3)_3$ solution without and with SO_4^{2-} ions. The presence of the SO_4^{2-} ions in the solution resulted in formation of the film, containing a larger amount of Ce and a higher amount of Ce(IV) in the conversion film. However, a low conversion films thickness and the presence of cracks yielded a lower level of steel corrosion protection.

EIS was applied to study the self-healing processes in protective coatings on carbon steel substrates. The increase of the low frequency impedance during immersion of the sample with a cerium film in a 0.5 M NaCl solution can be correlated to the active corrosion protection originating the self-healing of defects.

ACKNOWLEDGEMENTS

This research was supported by the Research Council of Lithuania under Grant No. MIP – 029-2013. The authors thank dr. R. Juškėnas (Centre for Physical Sciences and Technology, Institute of Chemistry) for his assistance performing XRD measurements.

Received 4 June 2015
Accepted 18 June 2015

References

1. D. B. Freeman, *Phosphating and Metal Pre-Treatment*, Woodhead-Faulkner Ltd., Cambrige, England (1986).
2. D. Weng, P. Jokiel, A. Uebleis, H. Boehni, *Surf. Coat. Technol.*, **88**, 147 (1996).
3. K. Ogle, A. Tomandl, N. Meddahi, M. Wolpers, *Corros. Sci.*, **46**, 979 (2004).
4. A. Tomandl, M. Wolpers, K. Ogle, *Corros. Sci.*, **46**, 997 (2004).
5. H. Konno, K. Narumi, H. Habazaki, *Corros. Sci.*, **44**, 1889 (2002).
6. Y. K. Song, F. Mansfeld, *Corros. Sci.*, **48**, 154 (2006).
7. K. Kurosawa, T. Fukushima, *Corros. Sci.*, **29**, 1103 (1989).
8. C. G. da Silva, I. C. P. Margarit-Mattos, O. R. Mattos, H. Perrot, B. Tribollet, V. Vivier, *Corros. Sci*., **51**, 151 (2009).
9. F. Manselfd, Y. Wang, H. Shih, *Electrochim. Acta*, **37**, 2277 (1992).
10. M. Debalà, L. Armelão, A. Buchberger, I. Calliari, *Appl. Surf. Sci*., **172**, 312 (2001).
11. J. Zhao, G. S. Frankel, R. L. McCreery, *J. Electrochem. Soc*., **145**, 2258 (1998).
12. B. R. W. Hinton, D. R. Arnott, N. E. Ryan, *Met. Forum*, **7**, 211 (1984).
13. B. R. W. Hinton, L. Wilson, *Corros. Sci*., **29**, 967 (1989).
14. R. G. Buchheit, S. B. Mamidipally, P. Schmutz, H. Guan, *Corros. Sci*., **58**, 3 (2002).
15. Y. Kobayashi, N. Yamashita, Y. Fujiwara, M. Yamashita, *J. Surf. Fin. Soc. Jpn.*, **55**, 276 (2004).
16. Y. Kobayashi, Y. Fujiwara, *Electrochim. Acta*, **51**, 4236 (2006).
17. B. A. Boukamp, *J. Electrochem. Soc.*, **142**, 1885 (1995).
18. W. Machu, *Die Phosphatierung*, Verlag Chemie (1950).
19. M. F. Montemor, A. M. Simões, M. J. Carmezim, *Appl. Surf. Sci.*, **253**, 6922 (2007).
20. A. J. Aldykiewicz Jr., A. J. Davenport, H. S. Isaacs, *J. Electrochem. Soc.*, **143**, 147 (1996).
21. M. A. Arenas, J. J. Damborenea, *Surf. Coat. Technol*., **187**, 320 (2004).
22. M. Hoang, A. E. Hughes, T. W. Turney, *Appl. Surf. Sci.*, **72**, 55 (1993).
23. G. Praline, B. E. Koel, R. L. Hance, H.-I. Lee, J. M. White, *J. Electron Spectrosc. Relat. Phenom.*, **21**, 17 (1980).
24. J. Z. Shyu, K. Otto, W. L. H. Watkins, G. W. Graham, R. K. Belitz, H. S. Gandhi, *J. Catal.*, **114**, 23 (1988).
25. X. Yu, G. Li, *J. Alloys Compd*., **364**, 193 (2004).
26. A. Pardo, M. C. Merino, R. Arrabal, F. Viejo, J. A. Muñoz, *Appl. Surf. Sci*., **253**, 3334 (2007).
27. M. L. Zheludkevich, R. Serra, M. F. Montemor, K. Y. Yaskau, I. M. Miranda Salvado, M. G. S. Ferreira, *Electrochim. Acta*, **51**, 208 (2005).
28. M. L. Zheludkevich, K. A. Yasakau, A. C. Bastos, O. V. Karavai, M. G. S. Ferreira, *Electrochem. Commun.*, **9**, 2622 (2007).

O. Girčienė, L. Gudavičiūtė, A. Selskis, V. Jasulaitienė, S. Šakirzanovas, R. Ramanauskas

CERIO OKSIDO SLUOKSNIŲ, NUSODINTŲ ANT ANGLINIO PLIENO, SAVAIMINIO UŽGIJIMO GEBA

S a n t r a u k a

Metalų aktyvi korozinė apsauga reiškia ne tik mechaninį paviršiaus padengimą, bet ir nusodintos dangos savaiminį užgijimą po jos pažeidimo (įbrėžimo). Darbo tikslas – ištirti ir parinkti bechromes konversines dangas ant anglinio plieno, pasižyminčias savaiminiu užgijimu po jų pažeidimo. Konversinių dangų struktūra, fazės bei cheminė sudėtis tirti SEM, XRD ir XPS metodais. Pasyvių sluoksnių apsauginės savybės nustatytos atliekant elektrocheminius tyrimus (voltamperometrija, EIS), savaiminis cheminės dangos užgijimas po įbrėžimo tirtas EIS metodu. Anglinio plieno ir fosfatuoto anglinio plieno paviršiai buvo modifikuoti Ce jonais nusodinant konversines dangas iš $Ce(NO_3)_3$ tirpalų. Tyrimai parodė, kad kai tirpale yra SO_4^{2-} jonų, gauta danga yra plonesnė, joje daugiau cerio ir mažai tirpių Ce(IV) junginių, tačiau sutrūkinėjusi ir todėl nepasižymi gera antikorozine apsauga. EIS tyrimai parodė, kad ilgėjant tiriamųjų pavyzdžių išlaikymo 0,5 M NaCl tirpale laikui yra stebimas žemų dažnių impedanso verčių padidėjimas, kurį lemia dangos aktyvi korozinė apsauga, t. y. savaiminis defektuotų vietų užgijimas.